Received 29 September 2023; accepted 24 October 2023. Date of publication 31 October 2023; date of current version 11 December 2023.

Digital Object Identifier 10.1109/OJAP.2023.3328813

Decoupling for Millimeter-Wave Array Antennas Using Near-Field Shrinking Dielectric Superstrate

SHENGYUAN LUO [1], YIMING ZHANG [2] (Member, IEEE), PENG MEI [1] (Member, IEEE), GERT FRØLUND PEDERSEN [1] (Senior Member, IEEE), AND SHUAI ZHANG [1] (Senior Member, IEEE)

[1] Antenna, Propagation, and Millimeter-Wave Systems Section, Aalborg University, 9220 Aalborg, Denmark

[2] Guangdong Provincial Key Laboratory of Optoelectronic Information Processing Chips and Systems, School of Electronics and Information Technology, Sun Yat-sen University, Guangzhou 510006, China

CORRESPONDING AUTHOR: S. ZHANG (e-mail: sz@es.aau.dk)

ABSTRACT A decoupling concept of near-field shrinking dielectric superstrate (NFSDS) is proposed for large-scale, wideband, and dual-polarized mm-wave arrays. An NFSDS with a thickness of 4 mm (0.32 λ_0 at 24 GHz) is mounted seamlessly above the array, which shrinks the near field of the array elements to reduce the space wave coupling while slightly increasing the surface wave coupling of the arrays. By loading a superstrate with a certain thickness and low permittivity, the total coupling of the mm-wave arrays is reduced significantly. Periodic air holes are drilled through the superstrate to lower the NFSDS permittivity. An 8 × 8 mm-wave array is simulated, fabricated, and measured to verify the proposed decoupling concept. The simulated and measured coupling of the mm-wave array is reduced from –17 dB to lower than –23.2 dB from 24–29.5 GHz and lower than –25 dB in most of the band, respectively. The radiation patterns of the array before and after decoupling almost keep unchanged. Moreover, the NFSDS can efficiently improve the array beam scanning capability. The measured results align well with the simulated.

INDEX TERMS Mutual decoupling, NFSDS, large-scale, mm-wave antenna array, space wave coupling, surface wave coupling.

I. INTRODUCTION

THE LARGE-SCALE mm-wave arrays is an important research topic that has attracted tremendous attention over the past few years [1]. Since the mutual coupling between array elements seriously deteriorates the performance of the arrays, such as active VSWR, bandwidth, active reflection coefficient, efficiency, signal-to-interference noise ratio, and channel capacity [2], [3], [4], [5], [6], [7], therefore, it is demanding to suppress the coupling of large-scale arrays.

Recent years have witnessed the efforts devoted to reducing the coupling of the arrays in the low-frequency bands, such as electromagnetic bandgap (EBG) [8], defected ground (DGS) [9], resonator [10], neutralization line [11] and parasitic element structure [12], which are commonly arranged between array elements. Thus, the inner-element distance needs to be large enough to accommodate the decoupling structure. The decoupling network is an effective method for mutual coupling suppression [13], which commonly operates within a narrow bandwidth. The metasurface is another effective decoupling method, which is typically loaded above the arrays with a distance [14], [15]. However, the mm-wave arrays are very sensitive to the distance between the metasurface and the array. Therefore, such a distance would affect the decoupling performance. A decoupling method of orthogonal feeding structure was proposed in [16]. However, it cannot be used in large-scale phased arrays either. A sub-6 GHz massive MIMO array with high isolation was proposed at the interface between medium and air in [17], yet the decoupling was led by the perturbation at the interface between medium and air, which introduces an air gap between medium and destroy the integrity of the medium. Reference [18] proposed a method of dielectric loading and covering in rectangular waveguide phased

arrays. It investigated the effect of dielectric geometry, constant, and sheath thickness on the wide scanning angle property of a rectangular waveguide phase array. In [18], the decoupling performance of the rectangular waveguide phase array was just simply studied and compared for the cases with different loaded dielectric parameters. However, the decoupling principle was not investigated in detail, especially the feasibility of decoupling for dual-polarization millimeter-wave arrays.

This paper firstly presents a decoupling concept of near-field shrinking dielectric superstrate (NFSDS) to reduce the coupling of large-scale, wideband, and dual-polarized mm-wave arrays, where the space wave coupling plays a decisive role. By employing the NFSDS, the space wave coupling of the mm-wave coupling could be significantly suppressed while the surface wave coupling slightly increases. But the total coupling of the array could have a decrement of 6.2 dB (from –17 dB to –23.2 dB) from 24 – 29.5 GHz and 7 dB (from –17 dB to –24dB) from 26.8 – 29.5 GHz. Compared to the currently existing literature, the novelty of the proposed decoupling method of NFSDS is summarized as follows:

1. The decoupling concept of near field shrinking is first proposed. The electromagnetic waves continuously propagate in NFSDS without perturbation, while the near field distribution is just shrunk to reduce the total coupling of the array.

2. Because the superstrate has a stable permittivity of 1.6 in a wide band, which is an intrinsic property of the superstrate itself. Hence, it can shrink the near field of the antenna itself without considering the coupling paths. Therefore, it can generally be applied in other massive MIMO array types.

3. The NFSDS is easy to integrate with mm-wave arrays, where the NFSDS has very simple structure and is mounted seamlessly above the mm-wave arrays. No air gap is introduced in actual applications to avoid fabrication errors.

This paper is organized as follows: Section II describes the decoupling principle in detail using a simple example of a dual-element array. The 8 × 8 decoupled mm-wave array was designed by applying the proposed decoupling concept of NFSDS. Section III presents antenna performance, including S-parameters, radiation patterns, beam scanning capability, realized gain, and total efficiency. Section IV concludes the paper.

II. PROPOSED DECOUPLING CONCEPT OF NFSDS

A. DECOUPLING SCHEME OF THE NFSDS

The sketch of the decoupling concept of NFSDS for mm-wave arrays is presented in Fig. 1. The coupling of array is composed of surface wave coupling component x1 and space wave coupling component x2, where the space wave coupling dominates with the inter-element distance close to half wavelength. It clearly demonstrates that the near fields of the array elements largely overlap with each other, which causes space wave coupling between array elements. When an NFSDS is seamlessly mounted above the array, the near-field electric field can be significantly shrunk, thereby reducing space wave coupling. The decrement of the space wave coupling is much larger than the increment of the surface wave coupling component x1'. Consequently, the total coupling of the array is still reduced significantly.

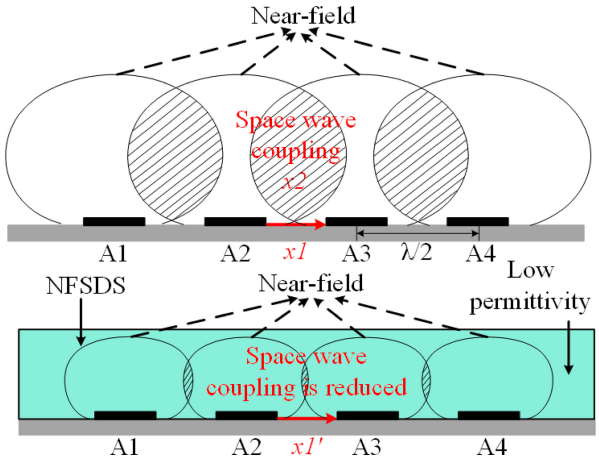

FIGURE 1. The decoupling sketch of the NFSDS.

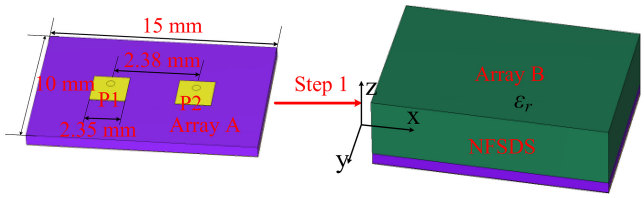

FIGURE 2. The analysis for the verification of the proposed decoupling concept.

B. VERIFICATION OF THE PROPOSED DECOUPLING CONCEPT

An analysis of the proposed decoupling concept is depicted in Fig. 2. A dual-element H-coupled patch antenna array working at 27 GHz is adopted as a reference, named Array A. The metal patches are printed on the top surface of the Rogers RO4350B substrate with a thickness of 1.52mm, a relative permittivity of 3.66 and a loss tangent of 0.0037. The center-to-center distance between array elements is around half-wavelength, and the patch size is 2.35 mm. Then, a pure superstrate with different permittivity and a thickness of 4 mm is mounted seamlessly above array A. The array with NFSDS is labeled as Array B.

Intuitively, the permittivity and the thickness of the NFSDS affect the amount of reduction in space wave coupling and increment in surface wave coupling of the mm-wave arrays. To better understand the effect of the permittivity ε_r and the thickness hs of the NFSDS on the decoupling level, the parametric study of the permittivity ε_r and the thickness hs has been carried out. As the permittivity ε_r varies from 1.3 to 2.2 at a step of 0.3, the E-fields of Array B at 27 GHz (mentioned in Fig. 2) are shown in Fig. 3, respectively. For the E-field distribution of Array A, a black rectangular frame is constructed and filled with electric

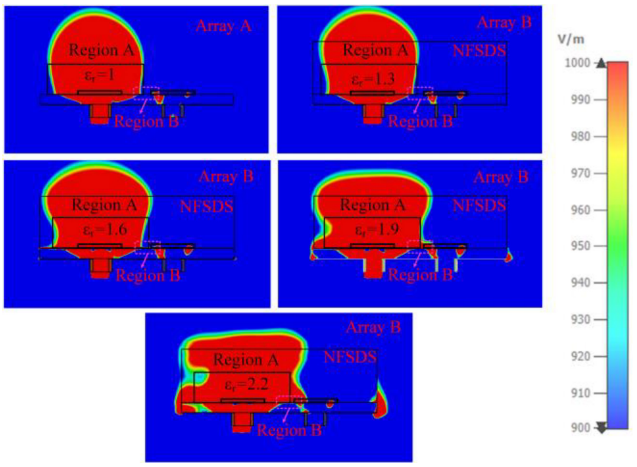

FIGURE 3. The E-field of the Array B with different ε_r varying from 1.2 to 2.1 at a step of 0.3 at 27 GHz.

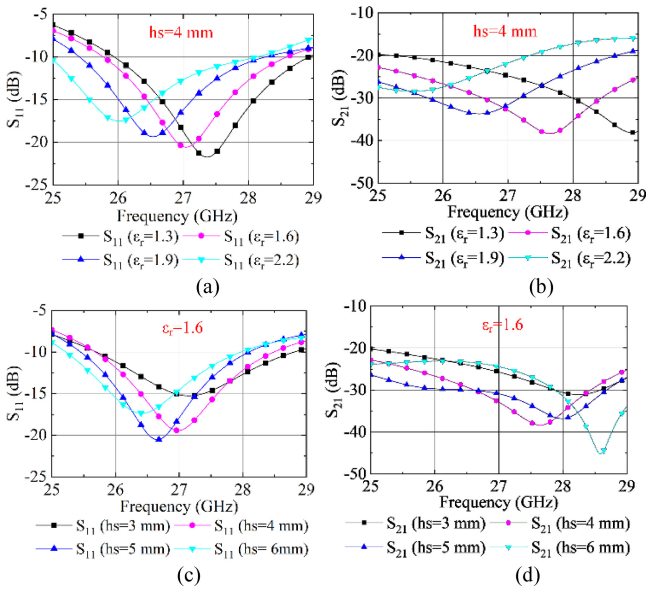

FIGURE 4. The S-parameters of the Array B with different ε_r varying from 1.2 to 2.1 at a step of 0.3, and hs varying from 3 mm to 6 mm at a step of 1 mm: (a) S11 of the Array B with different ε_r when hs is 4 mm, (b) S21 of the Array B with different ε_r when hs is 4 mm, (c) S11 of the Array B with different hs when ε_r is 1.6, (d) S21 of the Array B with different hs when ε_r is 1.6.

fields. However, in the same area of Array B, the edge of the E-field is far from the side of the black rectangular frame. It presents that the near field E-field in region A of Array B is smaller than that of Array A in the same area, demonstrating that the NFSDS can suppress the coupling of the array. The E-field distributions of Array B with different permittivity also show that when the permittivity ε_r increases gradually, the near field E-field distribution in Region A shrinks correspondingly, yet the surface wave coupling in region B increases.

The S-parameters of Array B with different permittivity ε_r are presented in Fig. 4 (a) and Fig. 4 (b), which have the same step as that in the procedure of the parametric study for E-fields. Fig. 4 (a) shows that the operating band of Array B shifts to a lower band as the increment of ε_r, which is caused by the change of the quality factor (Q value). Fig. 4 (b) demonstrates that as the permittivity ε_r is 1.6, the coupling of the Array B reaches the lowest level and less than –38.3 dB within the working band. Fig. 4(c) and Fig. 4(d) give the S11 and S21 of the Array B with different thicknesses of hs that vary from 3 mm to 6 at a step of 1mm, respectively. Fig. 4 (c) depicts that the working band of array B shifts to a lower band when hs increases, which also results from the quality factor (Q value) change. In addition, when the thickness hs is set as 4 mm (around half wavelength in the dielectric substrate), the coupling of the Array B is lower than 38.3 dB. Though the coupling of Array B with a thickness of 5mm is lower than that with a thickness of 4mm, its working band shifts toward a lower band than the required band. In the end, the permittivity and thickness of the NFSDS are optimized and set as 1.6 and 4 mm, respectively. Though the thickness of the NFSDS is relatively large, it is acceptable in mm-wave band application. Figure 3 and the parametric study results in Fig. 4 provide evidence that as a compromise value of ε_r is 1.6, the largest difference between space wave coupling reduction and surface wave coupling increment can be obtained. Thus, the lowest coupling of the Array B can be achieved.

III. DESIGN EXAMPLE

A. ANTENNA CONFIGURATION

An 8 × 8 mm-wave array with NFSDS is designed to verify the decoupling concept of NFSDS for large-scale, wideband, and dual-polarized mm-wave arrays. Fig. 5 presents the explosion structure and dimensions of the 8 × 8 mm-wave array element with NFSDS. The proposed array consists of dual layers of circle patches to generate two closed resonant frequencies to broaden the antenna working band. The array elements are fed by the differential feed structure. In the end, a dual-polarized array element with high port-to-port isolation can be obtained. Here, the inverting power divider of the differential feed structure has two arms (arm1 and arm2) with a length difference of half-wavelength at the center frequency to generate differential signals. In addition, practical base stations require a beam scanning capability more than 50° in x-direction, and a relatively small beam scanning capability more than 30°. Therefore, the array element distance in x-direction and y-direction are set as 5.2 mm (0.448 λ_0) and 6.8 mm (0.612 λ_0), respectively.

The detailed explosion diagram of the 8 × 8 mm-wave array element with NFSDS and the dimensions of the differential feed structures are depicted in Fig. 5 (a). The NFSDS is made of pure polypropylene (PP) with a dielectric constant of 2.2. Periodic air holes with a radius of rc, and a period of tp are drilled on it to get a lower effective permittivity. The thickness of the substrates, bonding files, and NFSDS are also given in Fig. 5 (a). The four metal probes pass through the circle slot on the ground and connect the differential feed structures with the bottom patch. The pad of the metal probes and the circle slot on the ground have a radius of rp and rs, respectively. TABLE 1 gives

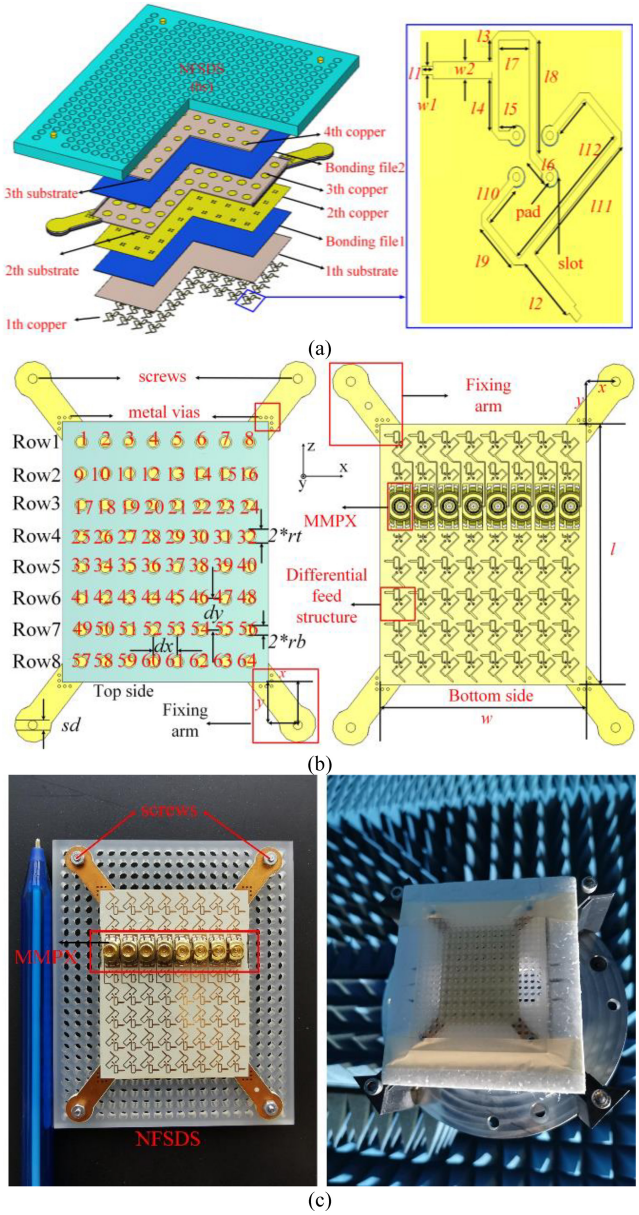

FIGURE 5. Configuration of the example: (a) the explosion structure of the 8 × 8 mm-wave array element with NFSDS and the detailed structure and dimensions of the feeding structure, (b) the specific geometry of the array without NFSDS from the top and bottom views and the arrangement of the mm-wave array and the feeding ports in −45° polarization, (c) the fabricated prototype of the Array with NFSDS.

the dimensions mentioned above. The specific geometry of the array without NFSDS arrangement of the mm-wave array and the feeding ports in –45° polarization is shown in Fig. 5 (b) from top and bottom view. The four fixing arms are connected to the corners of the substrate for installation. Here, the metal vias are drilled on the fixing arms to avoid the effect of fixing arms on antenna performance. Fig. 5 (c) gives the fabricated prototype of the array with NFSDS, where the NFSDS and the original array are seamlessly pressed together by four screws. The MMPX connectors feed the array. The common ground, bottom and top circle patches are printed on the Rogers RO4350B substrate, which are

TABLE 1. Parameters of the array with NFSDS.

	dx	*dy*	*hs*	*hs1*	*hs2*	*hs3*	*hb1*
Val.(mm)	5.2	6.8	4	0.10 1	0.33 8	0.50 8	0.20 2
Par.	***hb2***	***l***	***l1***	***l2***	***l3***	***l4***	***l5***
Val.(mm)	0.303	56.4	0.3	1.7	0.5	1.22	0.5
Par.	***l6***	***l7***	***l8***	***l9***	***l10***	***l11***	***l12***
Val.(mm)	0.72	0.88	2.74	1.3	1.1	3.55	3.96
Par.	***rb***	***rc***	***rp***	***rs***	***rt***	***sd***	***tp***
Val.(mm)	1.46	1.1	0.2	0.25	1.14	2	3
Par.	***w***	***w1***	***w2***	***x***	***y***		
Val.(mm)	43.6	0.2	0.4	6.8	9.2		

Val.: Value.

attached together by the bonding files to avoid air gaps. The bonding films used here are Rogers 4450F with a dielectric constant of 3.52 and a loss tangent of 0.004. Finally, the NFSDS covers the original array to shrink the near fields of the array elements. Even though the NFSDS and original array are not sticked together, there are no air gap between NFSDS and original array because pp board and Ro4350 are not easily deformed when they are screwed together. Additionally, the sizes of pp board and Ro4350 are very small, when the four corners of pp board and Ro4350 are pressured, their shape is basically kept unchanged. From Fig. 5 (d), we can know that due to the space limitation, only a row of MMPXs is connected to the array to activate the array elements in one polarization. Then, the array elements of the other rows are connected to the MMPX connector in turn so that the test can be smoothly implemented.

Here, two reasons cause the size of NFSDS to be larger than the size of the antenna:

1. The fixing arm is located outside the antenna array, and the hole, the screw passes through, is far away from the antenna array. Therefore, NFSDS should cover the fixing hole to facilitate installation and fixing.

2. To enable the NFSDS to cover the near field of the edge elements of the antenna array, the size of the NFSDS should also be larger than the size of the antenna array.

B. ANTENNA ARRAY PERFORMANCE

The S-parameters of the 8 × 8 mm-wave arrays before and after decoupling are simulated and measured. The reflection coefficient and the envelopes of the couplings of the array elements are depicted in Fig. 6. A high transmission coefficient indicates that a significant portion of the input power is radiated to the nonadjacent and adjacent array element, which leads to high mutual coupling between array elements. In terms of a certain array element, for example, A25, it has 127 coupling paths with other feeding ports. Then the maximum coupling value of every path is extracted varying the frequency to form the envelope of the coupling as seen in Fig. 6. For the other selected elements, the envelop

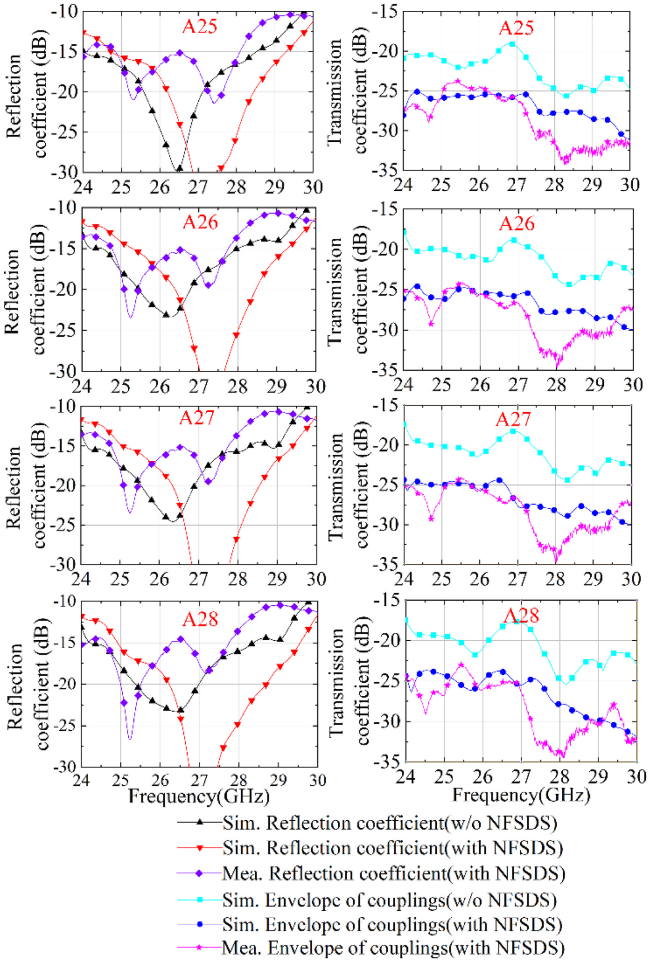

FIGURE 6. The reflection coefficient and transmission coefficient of the mm-waves array with and without NFSDS.

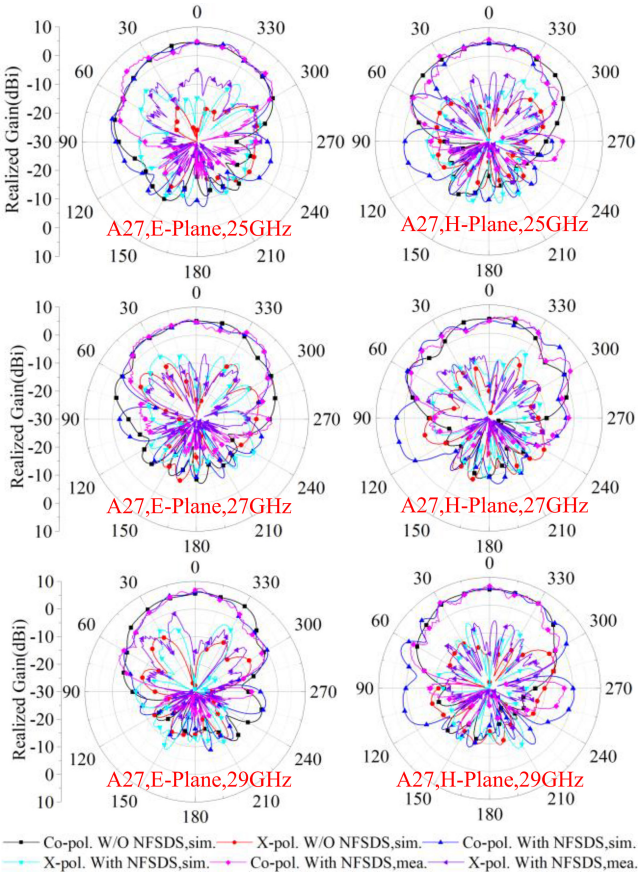

FIGURE 7. The radiation patterns of the mm-waves array element A27 before and after deploying NFSDS at 25GHz, 27GHz, and 29GHz.

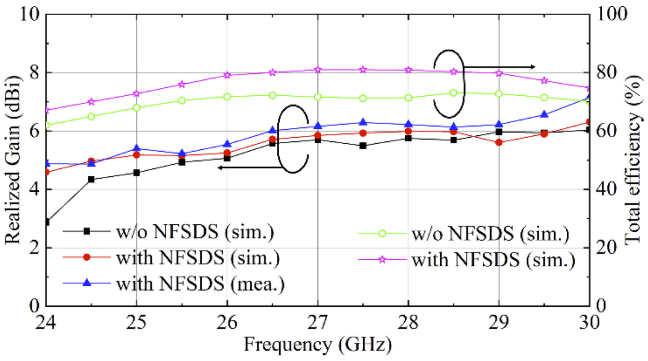

FIGURE 8. The realized gain and total efficiency of the array with and without NFSDS.

of the coupling can be extracted by adopting similar options. Notably, the coupling paths of this array includes coupling in x-direction, y-direction, diagonal direction between neighbor, non-neighbor array elements, and cross polarization ports of array element itself. The elements in the left part of the inner loop are selected because of the symmetry along the y-axis, including Row 4 (A25, A26, A27, A28). It demonstrates that the mm-wave array with NFSDS has a –23.2 dB and –24 dB decoupling bandwidth of 24 – 29.5 GHz and 26.8–29.5 GHz, respectively. The simulations and measurements illustrate that the NFSDS can effectively reduce the total coupling of the mm-wave arrays.

The radiation patterns of the array element A27 at 25 GHz, 27 GHz, and 29 GHz are presented in Fig. 7. The measurement for the radiation patterns is implemented in a chamber. There are some tiny distortions of the measured radiation patterns that makes the simulated and measured results are not matching so well, which are caused by the measurement tolerance. As seen in Fig. 5 (c), there is a metal plate in the microwave chamber to support our antenna, which introduces some reflection that causes the distortion of the measured radiation patterns. In addition, owing to our antenna works in mm-wave frequency. Therefore, some tiny measure tolerance will cause obvious mismatching with the simulated one. However, the contours of the radiation patterns of the mm-wave arrays before and after decoupling are unchanged within around –60° to 60° besides some sharp glitches, which illustrates that the loading of NFSDS almost does not affect the antenna performance.

Fig. 8 presents the realized gain and total efficiency of the selected element A27 at different frequencies. Here, the proposed decoupling method is applied for massive MIMO arrays, therefore the total efficiency of the array element

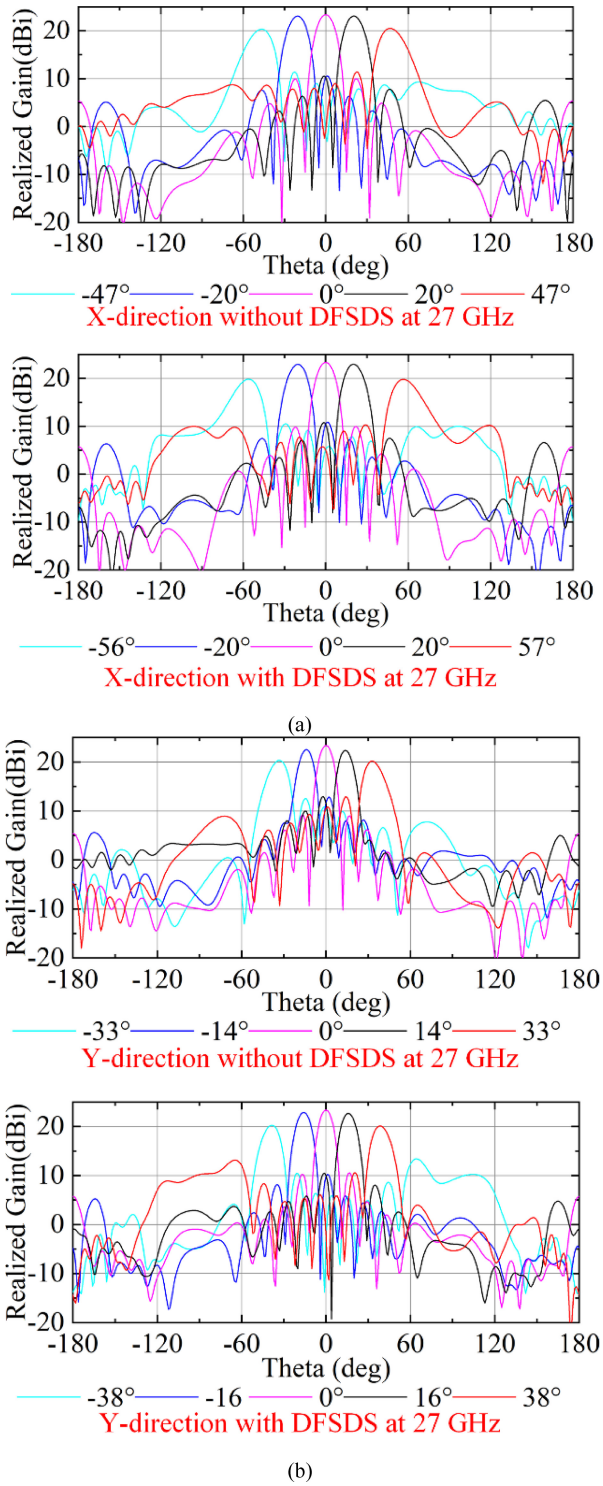

FIGURE 9. The beam scanning capability of the mm-wave array without and with NFSDS, (a) x-direction, (b) y-direction.

is given rather than the total efficiency of the array. Since the total coupling has a significant reduction, it means the electromagnetic wave radiated to other elements in the horizontal direction is reduced. Thus, the power radiated to the space is promoted. Consequently, the realized gain and total efficiency of the array elements are effectively improved by loading the NFSDS above the original array. Notably, according to the radiation patterns in Fig. 7, though the counter of the radiation patterns of the array with and without are basically same, some sharp distortion occurred after loading the NFSDS, which contributes to realized gain improvement. Here, the pink point of the realized gain appears at the sharp distortion. As a result, even though the counter of the radiation patterns before and after loading NFSDS are keep same, the peak realized gain has an increment by loading NFSDS. The results in Fig. 8 conform to the theoretical analysis from Fig. 8.

C. BEAM SCANNING CAPABILITY

The beam scanning capability is an important metric for large-scale phased arrays. Fig. 9 presents the simulated beam scanning of the mm-wave array with and without NFSDS in x-polarization and y-polarization, respectively. It can be found that the 3dB gain drop beam scanning capability of the original array in the x-direction and y-direction is –47°–47° and –33°–33°, respectively, while the decoupled array has a 3dB gain drop beam scanning capability of –56°–57° and –38°–38° in x-direction and y-direction, respectively. It concludes that the NFSDS can facilitate the beam scanning capability of the array. For the base stations, the beam scanning capability in y-direction is normally required no less than ±30°, while it requires a stronger beam scanning capability in x-direction than that in y-direction. Therefore, the proposed array in this paper can fully satisfy the industry requirement of the base station design.

IV. ANTENNA PERFORMANCE COMPARISON

The performance of the proposed array with NFSDS is compared with the structures in the current literature. The comparison is listed in TABLE 2. The methods of decoupling network and Array decoupling surface (ADS) [13], [14] are two effective decoupling approaches for massive MIMO arrays. However, it cannot be applied to mm-wave antennas. The TMS in [15] divides the space wave coupling into two parts with different propagation paths with the same amplitudes and opposite phases to enable cancellation with each other. Yet, owing to the decoupling performance of mm-wave arrays being sensitive to the distance between the array and metasurface, it is difficult to be used in mm-waves applications. In addition, the working band of the arrays in [13], [14], and [15] is narrower than the one in our work. The decoupling method in [16] can be used in mm-wave antennas. Although the antenna in [16] has a wider bandwidth than that in our work, its isolation improvement is caused by the orthogonal feed mode, and the best isolation reaches 17.6 dB, which is far lower than 23 dB.Notably, the 23 dB (in isolation) is selected as a benchmark is because that the distance between array elements is $0.448\lambda_0$ in x-polarization, which is smaller than the normal schedule of half wavelength. In addition, the proposed array of our work has the most stable reflection and transmission coefficient with the 23 dB isolation

TABLE 2. Performance comparison of the proposed antenna array with other similar work.

Ref.	Decoupling method	Pol. & Scale	Freq. (GHz) and Imp. BW (%)	23 dB Iso. BW (%)	Antennas Distance	Beam scanning (3dB gain drop)	Feasib. for mm-wave massive MIMO arrays
[13]	Decoupling network	Dua.-pol. 4 × 4	4.8-5 (4.08%)	2.04%	$0.50\lambda_0$	--	no
[14]	ADS	Dua.-pol. 4 × 4	3.2-3.9 (19.72%)	14.29%	$0.65\lambda_0$	--	no
[15]	TMS	Dua.-pol. 4 × 4	4.21-4.82 (13.51%)	13.5%	$0.5\lambda_0$	--	no
[16]	Orth. feed network	Dua.-pol. 2 × 2	24-40 (50%)	--	--	--	yes
[17]	DDS	Dua.-pol. 4 × 4	4.25-5.25 (20%)	10.5%	$0.485\lambda_0\times$ $0.485\ \lambda_0$	--	yes
This work	**NFSDS**	**Dua.-pol. 8 × 8**	**24-29.5 (20.37%)**	**20.37%**	$\mathbf{0.448\lambda_0\times}$ $\mathbf{0.612\ \lambda_0}$	-56° — 57° (x) -38° — 38° (y)	**yes**

Ref.: Reference Pol.: polarized Dua.: Dual Freq.: Frequency Iso.: Isolation Feasib.: Feasibility imp.: impedance orth.: orthogonal

bandwidth.The orthogonal feed structure has an apparent superiority for isolation enhancement, yet it cannot be scaled to the massive MIMO arrays. Though the height of this work is around half wavelength, the real thickness of the NFSDS is just 4 mm. In addition, the low permittivity substrate is obtained by simply drilling the periodic air cavities on the pure PP board and loading above the array without an air gap. Therefore, the proposed array with NFSDS performs a low design and fabrication complexity that almost does not introduce fabrication tolerance. The array in [17] can also be applied in massive MIMO mm-wave arrays, but it has a narrower 23 dB isolation bandwidth than that of our work. For the fabrication of the work in [17], it adopts 3D printing technology, but it might introduce air to the printing material so that leads to fabrication tolerance. Especially for the mm-wave array, the antenna performance and the decoupling are highly sensitive to the stability of the adopted material. It is worth noting that the proposed decoupled array has an excellent beam scanning capacity than other antennas in current literature. In summary, the method proposed in this letter is a promising candidate for mm-wave application.

V. CONCLUSION

A novel decoupling concept of NFSDS for wideband and dual-polarized large-scale antenna arrays is proposed. By comparing the E-field distributions of the array covered by the pure substrate with different permittivity, the decoupling principle is analyzed carefully. The optimized permittivity is 1.6 and the thickness of the NFSDS is 4 mm and then a significant space wave coupling is suppressed. Based on the theoretical analysis, a real example of an 8 × 8 array with NFSDS is simulated, fabricated, and measured correspondingly. The measurements keep consistent with the simulated results. The array with NFSDS has a 23.2 dB and 24 dB decoupling bandwidth of 24–29.5 GHz and 26.8–29.5GHz, respectively. Meanwhile, the array has an excellent beam scanning capability of –56°–57° in the x-direction and –38°–38° in the y-direction, respectively which makes the decoupling method of NFSDS a promising solution for the isolation improvement of the dual-polarization and wideband mm-wave arrays in 5G and beyond application.

REFERENCES

[1] L. Possenti, M. Barbiroli, E. M. Vitucci, F. Fuschini, M. Fosci, and V. Degli-Esposti, "A study on mm-wave propagation in and around buildings," *IEEE Open J. Antennas Propag.*, vol. 4, pp. 736–747, 2023.

[2] A. Dürr, M. Linder, D. Schwarz, and C. Waldschmidt, "Highly efficient angular array calibration based on the modal wave expansion technique," *IEEE Open J. Antennas Propag.*, vol. 2, pp. 938–948, 2021.

[3] R. L. Grove, J. Dall, and P. Leth-Espensen, "Mutual coupling and channel imbalance calibration of colocated MIMO radars," *IEEE Open J. Antennas Propag.*, vol. 3, pp. 511–522, 2022.

[4] D. M. Pozar, "A relation between the active input impedance and the active element pattern of a phased array," *IEEE Trans. Antennas Propag.*, vol. 51, no. 9, pp. 2486–2489, Sep. 2003.

[5] Z. Ying and D. Zhang, "Study of the mutual coupling, correlations and efficiency of two PIFA antennas on a small ground plane," in *Proc. IEEE Antennas Propagat. Soc. Int. Symp.*, Washington, DC, USA, Jul. 2005, pp. 305–308.

[6] R. Janaswamy, "Effect of element mutual coupling on the capacity of fixed length linear arrays," *IEEE Antennas Wireless Propag. Lett.*, vol. 1, pp. 157–160, 2002.

[7] K. H. Chen and J. F. Kiang, "Effect of mutual coupling on the channel capacity of MIMO systems," *IEEE Trans. Veh. Technol.*, vol. 65, no. 1, pp. 398–403, Jan. 2016.

[8] Z. S. He, C. Jin, S. An, L. Kong, and J. Liu, "Integrated-EBG ridge waveguide and its application to an E-band waveguide 32×32 slot array antenna," *IEEE Open J. Antennas Propag.*, vol. 1, pp. 456–463, 2020.

[9] A. Madni and W. T. Khan, "Design of a compact 4-element GNSS antenna array with high isolation using a defected ground structure (DGS) and a microwave absorber," *IEEE Open J. Antennas Propag.*, vol. 4, pp. 779–791, 2023.

[10] M. Li, X. Chen, A. Zhang, W. Fan, and A. A. Kishk, "Split-ring resonator-loaded baffles for decoupling of dual-polarized base station array," *IEEE Antennas Wireless Propag. Lett.*, vol. 19, no. 10, pp. 1828–1832, Oct. 2020.

[11] R. Liu, X. An, H. Zheng, M. Wang, Z. Gao, and E. Li, "Neutralization line decoupling tri-band multiple-input multiple-output antenna design," *IEEE Access*, vol. 8, pp. 27018–27026, 2020.

[12] M. Li and S. Cheung, "A novel calculation-based parasitic decoupling technique for increasing isolation in multiple-element MIMO antenna arrays," *IEEE Trans. Veh. Technol.*, vol. 70, no. 1, pp. 6242–6253, Jan. 2021.

[13] Y. Zhang, Q. Ye, G. F. Pedersen, and S. Zhang, "A simple decoupling network with filtering response for patch antenna arrays," *IEEE Trans. Antennas Propag.*, vol.69, no. 11, pp. 7427–7439, Nov. 2021.

[14] C. Wei, Z. Zhang, and K. Wu, "Phase compensation for decoupling of large-scale staggered dual-polarized dipole array antennas," *IEEE Trans. Antennas Propag.*, vol. 68, no. 4, pp. 2822–2831, Apr. 2020.
[15] S. Luo, Y. Zhang, G. F. Pedesen, and S. Zhang, "Mutual decoupling for massive MIMO antenna arrays by using triple-layer meta-surface," *IEEE Trans. Open J. Antennas Propag.*, vol. 3, pp. 1079–1089, 2022.
[16] X. Dai and K. Luk, "A wideband dual-polarized antenna for millimeter-wave applications," *IEEE Trans. Antennas Propag.*, vol. 69, no. 4, pp. 2380–2385, Apr. 2021.
[17] P. Mei, Y. Zhang, and S. Zhang, "Decoupling of a wideband dual-polarized large-scale antenna array with dielectric stubs," *IEEE Trans. Veh. Technol.*, vol. 67, no. 4, pp. 2828–2863, Apr. 2018.
[18] V. Galindo and C. P. Wu, "Dielectric loaded and covered rectangular waveguide phased arrays," *Bell Syst. Tech. J.*, vol. 47, no. 1, pp. 93–116, Jan. 1968.

SHENGYUAN LUO received the B.E. and M.S. degrees from the Harbin Engineering University in 2015 and 2019, respectively. He is currently working with Aalborg University, Denmark. His recent research interests include microstrip antennas, wideband antennas, millimeter-wave array antennas, and massive MIMO antenna arrays.

YIMING ZHANG (Member, IEEE) received the B.S. degree from Central China Normal University in 2008, and the M.S. and Ph.D. degrees from the University of Electronic Science and Technology of China in 2014 and 2019, respectively. His current research interests include MIMO antenna decoupling, single-channel full-duplex communications, and passive RF and microwave components.

PENG MEI (Member, IEEE) received the B.Eng. and M.Eng. (with the highest Hons.) degrees in electromagnetic fields and microwave technology from the University of Electronic Science and Technology of China, China, in 2015 and 2018, respectively, and the Ph.D. degree in wireless communications from Aalborg University, Denmark, in 2021.

He is currently working as an Assistant Professor with the Antennas, Propagation, and Millimeter-Wave Systems Section (AMPS), Department of Electronic Systems, Aalborg University, where he was a Postdoctoral Fellow with APMS Section in August 2023. His current research interests include periodic structures, metasurfaces, beam-steerable and 3-D printing antennas, transmitarray/reflectarray antennas, and reconfigurable intelligent surfaces. He was a recipient of the Excellent Master Thesis from the Chinese Institute of Electronics in 2019, and was invited to serve as a Session Chair for IEEE APWC in 2019, PIERS in 2022, ISAP in 2022, and PIERS 2023. He currently serves as the Chief Guest Editor for the special issue titled "Advanced Massive MIMO Antenna Arrays, Metasurfaces, and Reconfigurable Intelligent Surfaces for Sensing, Localization, and Wireless Communications" launched by *Sensors*, the Lead Guest Editor for the special section titled "Recent Advances on Absorbers/Rasorbers and Their Applications on Antennas and EMC" launched by IEEE OPEN JOURNAL OF ANTENNAS AND PROPAGATION, the Guest Editor for the article collection titled "Advancing Antenna Technologies for Mobile and Satellite Communications" launched by *Frontiers in Antennas and Propagation*, and the Best Paper Competition Co-Chair and an Organization Committee Member of the 2023 International Workshop on Antenna Technology held in Aalborg, Denmark, on 15–17 May 2023.

GERT FRØLUND PEDERSEN (Senior Member, IEEE) was born in 1965. He received the B.Sc. and E.E. (Hons.) degrees in electrical engineering from the College of Technology in Dublin, Dublin Institute of Technology, Dublin, Ireland, in 1991, and the M.Sc.E.E. and Ph.D. degrees from Aalborg University, Aalborg, Denmark, in 1993 and 2003, respectively. He was a Consultant for development of more than 100 antennas for mobile terminals, including the first internal antenna for mobile phones in 1994 with lowest SAR, first internal triple-band antenna in 1998 with low SAR and high TRP and TIS, and lately various multiantenna systems rated as the most efficient on the market. He has worked most of the time with joint university and industry projects and has received more than U.S. $21 million in direct research funding. He has been one of the pioneers in establishing over-the-air measurement systems. The measurement technique is now well established for mobile terminals with single antennas. Since 1993, he has been with Aalborg University, where he is currently a Full Professor with the Antennas, Propagation and Millimeter-wave Systems Laboratory with 25 researchers and the Head of the Doctoral School on Wireless Communication with 40 Ph.D. students enrolled. He is the Project Leader of the RANGE Project with a total budget of over U.S. $8 million investigating high-performance centimeter/millimeter-wave antennas for 5G mobile phones. He is currently involved in multiple-input and multiple-output (MIMO) OTA measurement. He has authored over 500 peer-reviewed papers, 6 books, and 12 book chapters, and holds over 50 patents. His current research interests include radio communication for mobile terminals, especially small antennas, diversity systems, propagation, and biological effects. He has chaired various COST groups with liaison to 3GPP and CTIA for over-the-air test of MIMO terminals.

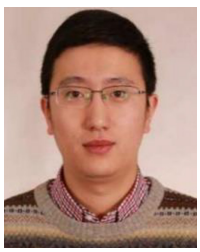

SHUAI ZHANG (Senior Member, IEEE) received the B.E. degree from the University of Electronic Science and Technology of China, Chengdu, China, in 2007, and the Ph.D. degree in electromagnetic engineering from the Royal Institute of Technology, Stockholm, Sweden, in 2013, where he was a Research Fellow. In April 2014, he joined Aalborg University, Denmark, where he currently works as an Associate Professor. From 2010 to 2011, he was a Visiting Researcher with Lund University, Sweden, and with Sony Mobile Communications AB, Sweden. He was also an External Antenna Specialist with Bang & Olufsen, Denmark, from 2016 to 2017. He has coauthored over 80 articles in well-reputed international journals and over 16 (U.S. or WO) patents. His current research interests includes mobile terminal mm-wave antennas, biological effects, CubeSat antennas, massive MIMO antenna arrays, UWB wind turbine blade deflection sensing, and RFID antennas.